Identifying the role of cytoplasmic Capping Enzyme in cellular recovery from oxidative stress

Synopsis of research

Submitted by

Anakshi Gayen

Enrollment number: PU/PHD/SBT/2020/003

Registration number: R-20RS220210316

Under the supervision of

Dr. Chandrama Mukherjee

Institute of Health Sciences

Presidency University

Kolkata

Name:	Ms. Anakshi Gayen
Supervisor:	Dr. Chandrama Mukherjee
Title of the thesis:	Identifying the role of cytoplasmic Capping Enzyme in cellular recovery from oxidative stress
PhD registration no.	R-20RS220210316
Enrollment number:	PU/PHD/SBT/2020/003
Place of work:	Institute of Health Sciences, Presidency University Plot No. DG/02/02, Premises No. 14-0358, Action Area-ID, New Town (Near Biswa Bangla Convention Centre) Kolkata 700156, West Bengal, India
Residential address:	CD 42, Sector 1, Salt Lake Kolkata- 700064
Communication address:	Institute of Health Sciences, Presidency New Town (Near Biswa Bangla Convention Centre) Kolkata 700156, West Bengal, India
Email:	anakshi.pf@presiuniv.ac.in gayenanakshi@gmail.com
Full signature of the scholar	Anakshi Gayen 20/01/2025
Full signature of the Supervisor	Chandrama Mukherjee 20/01/2025

Dr. Chandrama Mukherjee
Assistant Professor
Institute of Health Sciences
Presidency University, Kolkata

Declaration

I hereby declare that this synopsis of research contains original research work carried out by me under the guidance of Dr. Chandrama Mukherjee, Assistant Professor, Institute of Health Sciences, Presidency University, Kolkata, as part of the PhD programme.

All information in this document have been obtained and presented in accordance with academic rules and ethical conduct.

I also declare that, as required by these rules and conduct, I have fully cited and referenced all materials and results that are not original to this work. I also declare that, this work has not been submitted for any degree either in part or in full to any other institute or University before.

Anakshi Gayen
20/01/2025

Contents

Introduction…… 1

Hypothesis and objectives…… 2

Methods…… 2

Plasmid constructs…… 2

Cell culture and treatments…… 2

Plasmid and siRNA transfection…… 3

Whole, cytoplasmic and mitochondrial protein isolation…… 3

Stress granule isolation…… 3

Immunoprecipitation…… 3

Streptavidin pulldown…… 4

Western blotting…… 4

Indirect immunofluorescence…… 4

Cytoplasmic RNA preparation for RNA seq…… 4

polyA selection and XRN1 susceptibility assay…… 5

Selection of genes and validation by RT-qPCR…… 5

Domain wise full length docking of eIF3b and CE and MD simulation of docked complex 5

Statistical analysis…… 6

Results…… 7

Objective 1: Does cytoplasmic CE localize to stress granules?…… 7

Objective 2: Does CE affect the dynamics of SG formation?…… 11

Objective 3: Is CE-SG association regulated by VDACs?…… 15

Discussion…… 17

Bibliography…… 19

Introduction

The mRNA capping enzyme (CE) is essential in eukaryotic cells for processing mRNA, miRNA and other non-coding RNAs by adding a reverse 5'-5' triphosphate linkage to the first transcribed nucleotide. Though initially identified as a protective measure for viral mRNAs[1], but it is present in different domains of life encompassing yeast[2], trypanosomes[3] and mammals[4]. The cap, 7-methylguanosine is attached by removing one phosphate from the 5' triphosphate end of the nascent mRNA followed by covalent addition of GMP attached to lysine 294. Then, the RNA methyltransferase (RNMT) methylates the guanine forming the m7G cap. This canonical cap protects RNAs from degradation, enables their export from the nucleus, facilitates translation initiation by ribosomes in the cytoplasm, and dictates the RNA metabolism. In addition to cap, other epigenetic modifications, like methylation also dictate the fates of RNA [5,6]. RNA turnover is an important aspect of RNA metabolism. Decapping enzymes such as DCP1/2 cleave the terminal diphosphates and leave the monophosphorylated transcripts susceptible to exoribonucleases such as XRN1. Previously, it was believed that cap removal via decapping pathways would result in irreversible transcript degradation. Though early evidence demonstrated stable decay intermediate of beta-thalassaemic mRNA in the cytoplasm of erythroid cells of transgenic mice [7], it was Otsuka et al., who first identified the stable decay intermediate of mRNAs attain a cap onto the 5'-end in the cytoplasm[8]. In the cytoplasm, CE forms a large protein complex, termed as cytoplasmic capping complex (cCC) where cytoplasmic CE (cCE) relies on an adapter protein Nck1 and is essential for its recruitment and stabilization[9]. cCE has a diverse set of mRNAs[10] and long non-coding RNAs[11] as targets. Early evidence indicated that overexpression of the catalytically inactive form of capping enzyme, where the lysine residue at the active site is substituted with alanine (K294A), in the U2OS cell showed a poor recovery from oxidative stress[8].

In oxidative stress**,** reactive-oxygen-species (ROS) are generated**,** which evolves from both biotic and abiotic conditions and these are natural byproducts of normal metabolic processes that fuel various cellular functions but abnormal production can lead to different pathophysiological conditions. However, excessive accumulation of ROS culminates in the formation of dynamic membrane-less condensates in the cell termed stress granules (SGs), the cellular compartments that assemble only upon stress, play a cytoprotective role, and disassemble after stress removal[12]. Apart from oxidative stress, heat or nutrient stress also lead to the formation of SGs. SGs consist of translation initiation factors, mRNAs and various RNA binding and other proteins that coalesce together to phase out of the cytoplasm and play important role in many human diseases ranging from neurodegeneration, metabolic disorders, and cardiovascular diseases to cancer[13,14,15]. Another ribonucleoprotein foci are also found in the cytoplasm termed as processing bodies (PBs), spontaneously expressed and are the primary location of mRNA storage and degradation as these aggregates contain enzymes such as XRN1, DCP1[12]. Studies have shown that, mRNAs sequestered to SGs nearly completely disassemble upon stress removal and enter in active translation process[16]. After stress removal, the mRNAs enter translation, thereby maintaining homeostasis and

restoration of cap dependent translation may help in recovery from stress. These findings led us to think that cCE must have a specific role in the cytoplasm.

Hypothesis and objectives:

We propose that, cCE mediates cellular recovery from stress through recapping of target transcripts. The hypothesis has been verified by following aims.

1. Does cytoplasmic CE localize to stress granules?

2. Does CE affect the dynamics of SG formation?

3. Is CE-SG association regulated by VDACs?

Methods:

Plasmid constructs

Mammalian expression constructs of CE, bio-myc or myc-tagged CE-wt, CE-ΔTPase which were inserted into mammalian expression plasmid pCDNA3 using suitable restriction sites were, either by traditional cloning or using or Infusion HD cloning kit, used in the study. Myc tagged CE-wt in pLVX Tet-on puro and bio-myc K294A in pCDNA4TO were used to prepare U2OS stable cell line utilising puromycin and zeocin as selectable markers respectively. For VDAC constructs, expression vector pECE-3XHA was used to insert individual genes via infusion cloning. Dr. Nancy Kedersha (Harvard Medical School, USA) and Dr. Somshubhra Nath (Presidency University, India) generously provided us the GFP-G3BP1 and Rennila Luciferase construct respectively.

Cell culture and treatments:

U2OS (ATCC), NIH3T3 (TAKARA), HEK293, and RPE1 (ATCC) cells were maintained in Dulbecco's modified Eagle's medium (Invitrogen) with 10% FBS (Himedia) and 1% penicillin-streptomycin (Invitrogen). For stable cell lines, tetracycline negative FBS was used to maintain the cells. To induce oxidative stress, the cells were exposed to 0.5 mM sodium arsenite (NaAsO2) (Merck) for 1 hour. Recovery from was initiated by substituting the arsenite-containing medium with fresh, media and incubated for an additional 2 to 6 hrs. Cell viability was assessed using the XTT assay kit (Cell Signaling Technology) with measurements taken using a BioTek Synergy microplate reader. To inhibit transcription, 10 μM DRB (5,6-dichloro-1-β- d –ribofuranosylbenzimidazole) was administered to the cells for the mentioned duration.

Plasmid and siRNA transfection:

For microscopy assays, U2OS cells were plated at a density of 1.5×10^5 in 35 mm dishes. For western blot analysis, HEK293 cells were seeded at 2.5×10^5 and 6×10^5 in 35 and 60 mm dishes respectively. The JetPRIME transfection reagent (Polyplus) was utilized for the transfection of expression plasmids. For siRNA treatment, U2OS cells were seeded at 7.5×10^4 in each 35 mm dish and 2×10^3 in each well of a 96-well plate. The cells were transfected with siRNA targeting CE, eIF3B, VDAC1, VDAC2 or VDAC3 (Ambion) using Lipofectamine RNAiMAX (Invitrogen). A Silencer negative control (Ambion) was employed as a control for the siRNA transfection.

Whole, cytoplasmic and mitochondrial protein isolation

To isolate whole cell fraction, U2OS or HEK293 cells were harvested and lysed in whole cell lysis buffer (25 mM Tris-HCl, pH 8, 150 mM NaCl, 2 mM $MgCl_2$, 1% NP40 supplemented with 1 mM PMSF, 1X protease inhibitor cocktail). For cytoplasmic fraction, cells were harvested and lysed in cytoplasmic lysis buffer (20 mM Tris-HCl, pH 7.5, 100 mM NaCl, 10 mM $MgCl_2$, 10 mM KCl, 0.2% NP40 supplemented with 1 mM PMSF, 1X protease inhibitor cocktail). Mitochondria isolation was done from HEK293 cell using mitochondria isolation kit (Qiagen). Total protein was quantified using BCA rapid gold protein quantification kit (Thermo).

Stress granule isolation:

Stress granules were extracted from the cytoplasmic fractions of U2OS cells in accordance with the methodology outlined in Wheeler et al.[17], resulting in sub-fractions that included SG-enriched fractions and SG-depleted cytoplasm. The effectiveness of SG enrichment was assessed through immunoblotting utilizing antibodies specific to stress granule proteins. Cytoplasmic extracts from non-stressed cells served as a control. Cytoplasmic fraction of stress recovered cells was also analyzed.

Immunoprecipitation:

The cytoplasmic extract was used for immunoprecipitation (IP) utilizing ProteinG magnetic beads. After equilibration with IP buffer (25 mM Tris-Cl, pH 7.5, 150 mM NaCl) beads were incubated with 2 µg of anti-CE antibody for 1-hour followed by a 30-min blocking with a blocking buffer (1% BSA in IP buffer) at room temperature. The antibody-coated beads were then mixed with the pre-cleared cytoplasmic extract and incubated overnight at 4°C in shaking. The beads used for pre-clearing served as the negative control. Both the control and antibody-bound beads were washed with IP wash buffer (0.1% NP40 in IP buffer) followed by sample preparation.

Streptavidin pulldown:

Buffers used in immunoprecipitation were also used for pulldown of cytoplasmic and mitochondrial extracts. 10µl of streptavidin-Dynabeads (Invitrogen) were used for each sample. Equilibrated and blocked streptavidin beads were mixed with cellular extracts and binding was performed for 2.5 hrs. at 4˚C at shaking condition. Beads were then washed and prepared samples were subjected to immunoblotting.

Western blotting:

Protein samples prepared from cellular extracts, immunoprecipitated or pulldown complexes after mixing with Laemmli buffer were subjected to SGS-PAGE analysis followed by transfer onto nitrocellulose or Immobilon-FL PVDF membranes. After blocking with 3% bovine serum albumin in phosphate-buffered saline (PBS), membranes were incubated overnight at 4°C with primary antibodies diluted in the blocking buffer. Following PBS-T washing, the membranes were incubated in secondary antibodies, which were either Alexa Fluor 680-conjugated donkey anti-Rabbit (Invitrogen) and DyLight 800-conjugated donkey anti-mouse or anti-Goat (Invitrogen) at 1:10000 dilutions in PBS-T. The immunoblots were scanned using Odyssey CLx/Dlx infrared imaging system, and the background-corrected intensities of bands were determined using ImageStudio (Li-cor).

Indirect Immunofluorescence (IF):

For IIF assays, cells were grown on glass coverslips. After transfection and/or treatments, cells were fixed with freshly prepared fixing solution containing 4% paraformaldehyde (EMS) supplemented with 0.2% TritonX-100 (Biorad) in 1X PBS for 10 min at room temperature. After washing in 1X PBS containing 0.5 mM $MgCl_2$ and 0.05% Triton X-100, cells were incubated in a blocking buffer (5% FBS, 0.2 M glycine, 0.1% TritonX-100 in 1X PBS) for 30 min at room temperature. The cells were then incubated with the primary antibody diluted in blocking buffer overnight at 4°C. After washing, the cells were incubated with donkey anti-rabbit, donkey anti-goat, or donkey anti-mouse secondary antibodies conjugated with either Alexa Flour 488 (Invitrogen) or Alexa Fluor 568 (Invitrogen) (1:1000), and Hoechst 33358 diluted in the blocking buffer, for 45-60 min at room temperature. The coverslips were mounted on glass slides using slowfade mounting media (Invitrogen). Images were obtained using Confocal laser scanning microscope (Leica) fitted with a 63X Plan Apo oil immersion objective (NA 1.4).

Cytoplasmic RNA preparation for RNA seq

For RNA sequencing, two cell lines were used. U2OS cells stably expressing TetR that served as control and U2OS cells stably expressing bio-myc-K294A. Bio-myc-K294A was maximally induced using 1µg/ml

doxycycline for 24 hrs. Stress and recovery were performed as mentioned previous. Cytoplasmic RNA was isolated using TRizol (Invitrogen) and subjected to RNA sequencing.

polyA selection and XRN1 susceptibility assay

Cytoplasmic RNA isolated form different cytoplasmic extracts and 2μg of each RNA was subjected to polyA selection using Dynabeads mRNA Direct purification kit (Invitrogen). PolyA selected RNAs were mixed with synthetic uncapped GFP spike-in and synthetic capped renilla luciferase at a dilution of 1:1000 and incubated with or without XRN1(NEB) for 1.5 hr. RNA was purified using phenol:chloroform:isoamyl alcohol (SRL) followed by ethanol precipitation.

Selection of genes and validation by RT-qPCR

From RNA sequencing analysis, genes were selected with p value <=0.05 and fold change≥2, which are differentially expressed in recovery condition and are related to diabetes mellitus. To validate the result, RNA was extracted and cDNA was synthesized using iScript cDNA synthesis kit (Biorad) and qPCR reactions were performed with SsoAdvanced Universal SYBR Green Supermix (Biorad) using CFX connect Real-Time instrument (Biorad). Similarly, following XRN1 susceptibility assay, RT-qPCR was done using the purified RNA. The C_t values for target mRNAs and non-target controls were normalized against the C_t value of capped Renilla luciferase and the susceptibility was calculated by taking the ratio of normalized K294A samples to the control ones. Quantification was done either in Graphpad prism or in microsoft excel.

Domain-wise and full length docking of eIF3b and CE, and MD simulation of docked complex

The 3D structures of nine-bladed beta-propeller (PDB id: 4NOX) and RRM domain (PDB id: 2NLW) of human eIF3b, and 5'-triphosphatase (PDB id: 2C46) and RNA guanyltransferase (PDB id: 3S24), domains of human CE protein were obtained from the protein databank (PDB). Each of the eIF3 domain was docked with every CE domains using PatchDock[18], ClusPro[19] and HDOCK[20] programs. Among the 100 selected solutions of each pair, 30 generated docking solutions. These were subjected to root mean square deviation (RMSD) based clustering using UCSF chimera program. The largest cluster of each pair was ranked based on the score and compared to identify probable interaction pairs.

Next, the 3D structures of full length eIF3b (Id: AF_P55884_F1) and CE (Id: AF_O60942_F1) were extracted from AlfaFold database[21]. The unstructured regions were removed from eIF3b and then the truncated and full length eIF3b were docked using HDOCK. RMSD clustering was done for top 100 solutions and the MD simulation was run with the highest docking score of largest cluster. The eIF3b-CE complexes (before and after simulation) were validated by estimating the true like complex probability

at PCPIP (Protein Complex Prediction by Interface Properties) server[22] and MM/GBSA based binding energy estimation by Molecular mechanics with generalized Born and surface area solvation (MM-GBSA) module of HawkDock server[23] (Performed in the lab of Dr Saikat Chakrabarti, CSIR-IICB TRUE campus).

Statistical Analysis

The data were analyzed using Graphpad prism software or microsoft excel. One-Way ANOVA (Tukey's multiple comparison test) was performed to determine the statistical significance followed by student's two-tailed unpaired t-test. P-value below 0.05 was considered as significant (*P <0.05, **P <0.01, ***P <0.001, 'ns' refers to non-significant).

Results:

Objective1: Does cytoplasmic CE localize to stress granules?

CE is present in the cytoplasm and is a bonafide component of SG

CE was thought to be present only in the nucleus until the discovery of a cytoplasmic pool of capping enzyme. In our study, we showed that a significant amount of cCE is present in different primary cells

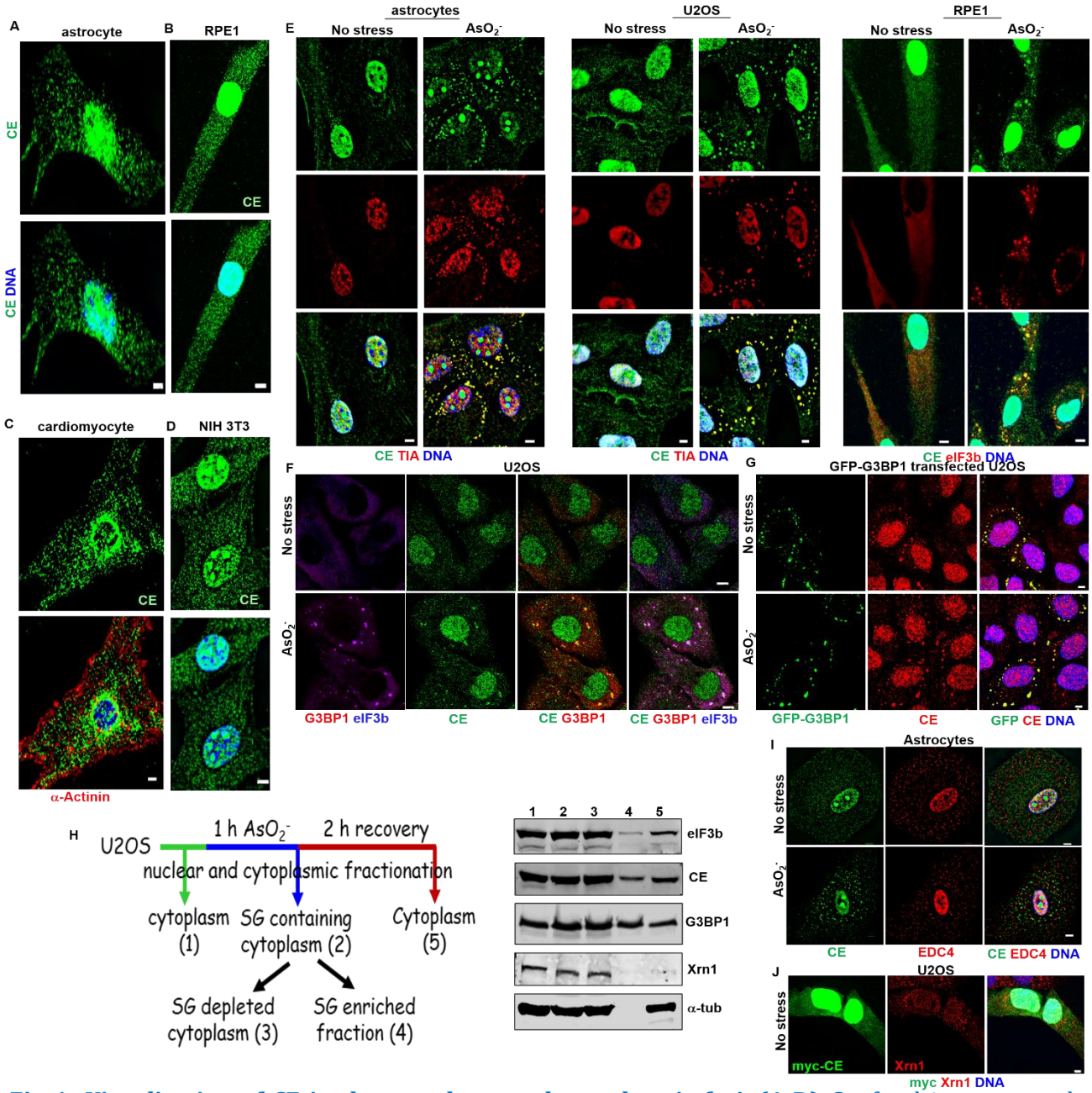

Fig 1. ***Visualization of CE in the cytoplasm and cytoplasmic foci***: **(A-D)** Confocal immunograph of different primary cells and lines of cells with endogenous CE. **(E-F)** Immunostaining of sodium arsenite treated different primary and lines of cells with CE and SG markers eIF3b, TIA and G3BP1. **(G)** Confocal immunograph of GFP-G3BP1 transfected cells with and without sodium arsenite treatment. **(H)** Scheme of SG isolation and Immunoblot analysis of biochemically isolated SGs. **(I-J)** Immunostaining of astrocytes and U2OS with EDC4 and XRN1 respectively to visualize CE in PBs. Bar represents 5 μM.

(astrocytes, cardiomyocytes) (Fig 1A, 1C) and lines of cells (RPE1, NIH3T3) (Fig 1B, 1D) by immunostaining of endogenous CE. Since previous studies showed that, expressing K294A in the cytoplasm results in the poor recovery of cells exposed to 0.5 mM sodium-arsenite introduced-stress, we investigated the localization of cCE in same condition. When cells are challenged to oxidative stress, they form SGs corroborated by immunostaining of CE with different SG markers such as eIF3b, G3BP1 and TIA (Fig 1E-F). In our study, we used eIF3b as the SG marker throughout our future experiments. To substantiate that cCE indeed is a bonafide component of SG, we checked with an SG nucleating protein G3BP1 (Ras GTPase-activating protein-binding protein 1), where overexpression of G3BP1 forms SG without the introduction of oxidative stress and the localization of cCE into the G3BP1 positive SGs were identified (Fig 1G). SGs were also isolated biochemically from U2OS cells and distribution of cCE was analysed in various cytoplasmic fractions (Fig 1H). We also examined if cCE localizes to P-bodies (PBs), which share certain components with SGs[24]. We have seen that, under any circumstances, non-stress and arsenite-induced stress, cCE does not colocalize with PBs (Fig I-J).

cCE interacts with eIF3b

An evolutionarily conserved protein eIF3b is a subunit of multi-protein complex eIF3 that is one of the complex translation initiation factors in mammals[25]. It is involved in almost every process of translation initiation in a cap-dependent manner and a core component of oxidative stress-induced SGs as a consequence of translational arrest[26]. A protein interactome analysis utilizing proximity-dependent biotin identification (BioID) identified eIF3b as an interactor of cCE among other RNA-binding proteins[27]. Based on this information, we sought to check whether eIF3b mediates the localization of CE to the SGs. To determine this, first an in-silico molecular docking approach utilized for domain-wise protein-protein interaction analysis. 3D structures of the domains of eIF3b and CE were extracted from protein data bank and were utilized for protein-protein docking (Fig 2A) using the PatchDock[18] (Fig 2B), HDOCK[20,28] (Fig 2C) and ClusPro[19] (Fig 2D) programs. The most favored interaction was observed between beta-propeller (BP) domain of eIF3b and 5'-triphosphatase (Phospho) and RNA guanyltransferase (GT) of CE (Fig 2G). After this, a full-length docking of eIF3b and CE taking 3D structures from Alphafold database, followed by molecular dynamics simulation-based stabilization was done (Fig 2E-F). Improvement in the binding energy post simulation compared to the pre-simulation indicates a stable interaction between the domains. The post-simulation validation using the Protein Complex Prediction by Interface Properties (PCPIP) server [22] showed a high probability (85-95%) of this protein-protein complex.

After in-silico validation, we sought to determine the same in *in vivo* system, specifically in oxidative stress condition by employing CE immunoprecipitation (IP). Cytoplasmic fractions from non-stress and 1 hr arsenite stress conditions were taken from U2OS cells and were subjected to

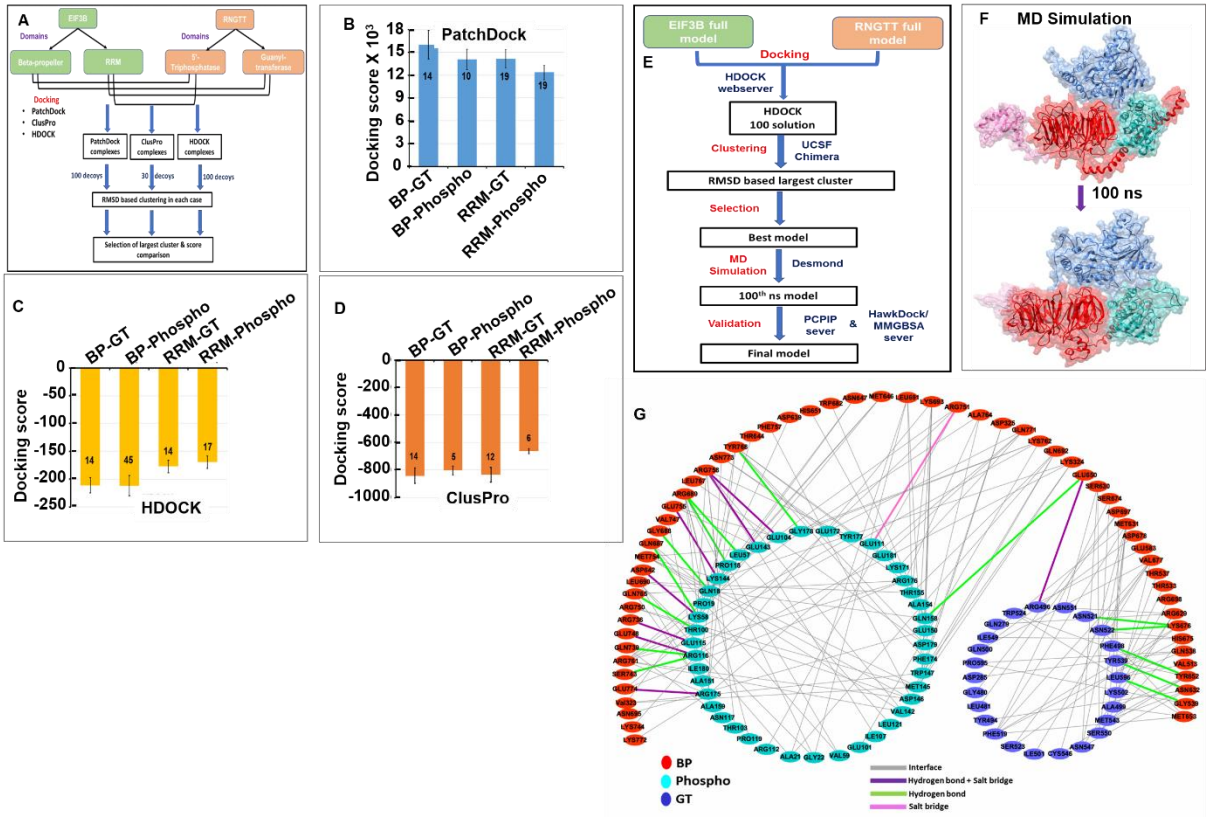

Fig2. ***In-silico molecular docking analysis between CE and eI3b***: **(A)** Scheme of domain-wise docking of CE and eIF3b using using PatchDock, HDOCK and ClusPro softwares. **(B-D)** Docking scores between different domains of CE and eIF3b. **(E)** Scheme of full length docking between the 3D structures of eIF3b and CE. **(F)** A full length docking of eIF3b and CE by molecular dynamics simulation based stabilization. **(G)** A model of probable interacting residues between the domains of eIF3b and CE with their types of interaction

immunoprecipitation using anti-CE antibody coupled proteinG beads. 3% Input (cellular fraction) and 100% recovered protein (from beads) were analysed by Western blot analysis. We observed that, in both non stress and arsenite stress conditions, eIF3b strongly interacts with cCE (Fig 3A), where the recovery of eIF3b with cCE in arsenite stress condition showed more when compared to the non-stress one (Fig 3B). This observation corroborated our *in-silico* data, indicating that the interaction is occurring in the cytoplasm. This implies eIF3b might be helping the recruitment of cCE into the SGs.

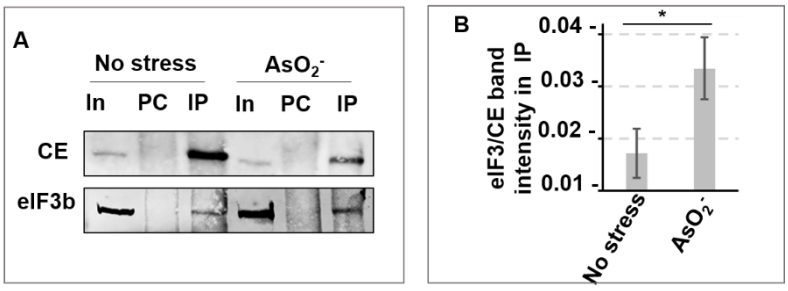

Fig3. ***In vivo interaction between CE and eIF3b***: **(A)** Immunoprecipitation using anti-CE antibody taking cytoplasmic fractions from non-stressed and arsenite stressed U2OS cells. eIF3b was checked as Co-IP. **(B)** Relative intensity of eIF3b to CE in immunoprecipitation was checked in arsenite treated cells compared to the control one.

Depletion of eIF3b reduces SG formation and cCE recruitment to SGs

Since our study already has showed interaction between cCE and eIF3 in both non-stress and oxidative stress conditions, we were intrigued to investigate the localization of cCE in eIF3b depleted state. A ~90% depletion of eIF3b leads to decrease in translations by treating the HCT116 cells with 500 μM indole-3-acetic acid for 24 hrs[29]. Additionally, >90% decrease in eIF3b level from osteosarcoma U2OS cells significantly reduces the cell viability[30]. So, to unperturbed cell viability, we depleted eIF3b from U2OS cells using 20nM siRNA against eIF3b where more than 50% reduction in total eIF3b was observed (Fig 4A) and checked the SG assembly. As expected, SG formation was compromised (Fig 4B). When checked with another SG marker G3BP1, we found that almost 100% eIF3b and G3BP1 localize to the same SG (Fig 4B). Reduction of eIF3b protein reduces overall formation and size of SGs as compared to control as evidenced by both eIF3b and G3BP1 marked SGs (Fig 4B-C). We also observe a reduced localization of cCE to the SGs in eIF3b depleted state while the cytoplasmic localization of CE remained unaltered. This data suggests that eIF3b is required for SG formation and cCE is only localized to SGs in presence of SG core proteins like eIF3.

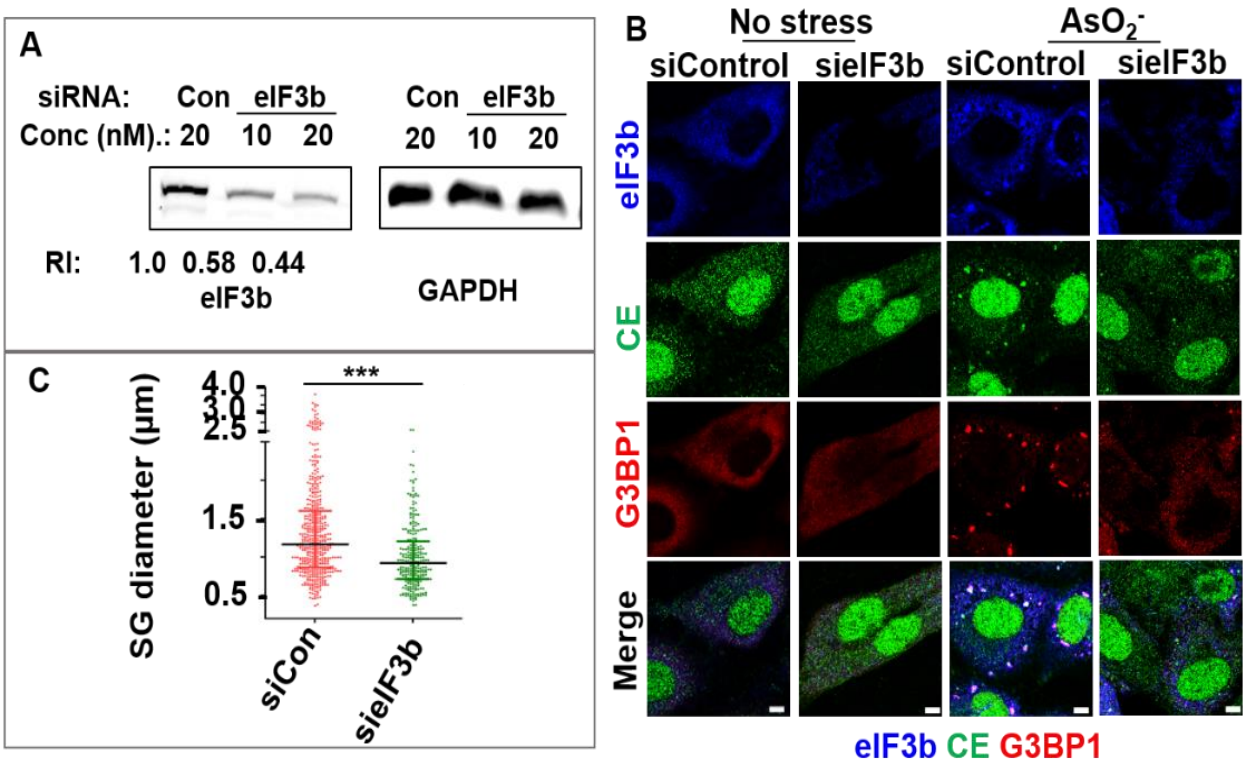

Fig4. ***Formation of SG and localization of cCE in eIF3b depleted cells***. **(A)** Immunoblot analysis for the validation of siRNA against eIF3b in U2OS cells. GAPDH had been used as loading control. **(B)** Confocal immunograph showing reduced formation of SGs and less cCE localization to SGs upon depletion of eIF3b from cells. G3BP1 was used as another SG marker. Bar represents 5 μM. **(C)** A dotplot showing reduced size of SG in eIF3b depleted cells when compared to the control.

Objective2. Does CE affect the dynamics of SG formation?

CE depletion has no role in SG assembly

Ribonucleoprotein (RNP) granule play pivotal roles through a unique spatiotemporal regulatory mechanism that carry out different physiological processes and mediate stress responses. We have already shown that cCE does not localize to PB puncta (Fig 1I-J) but is a bonafide component of SG (Fig 1E-G). We also observed localization of CE to SGs was reduced in eIF3b-depleted cells (Fig 4B). These observations prompted us to investigate whether CE has any involvement in SG formation. To examine,

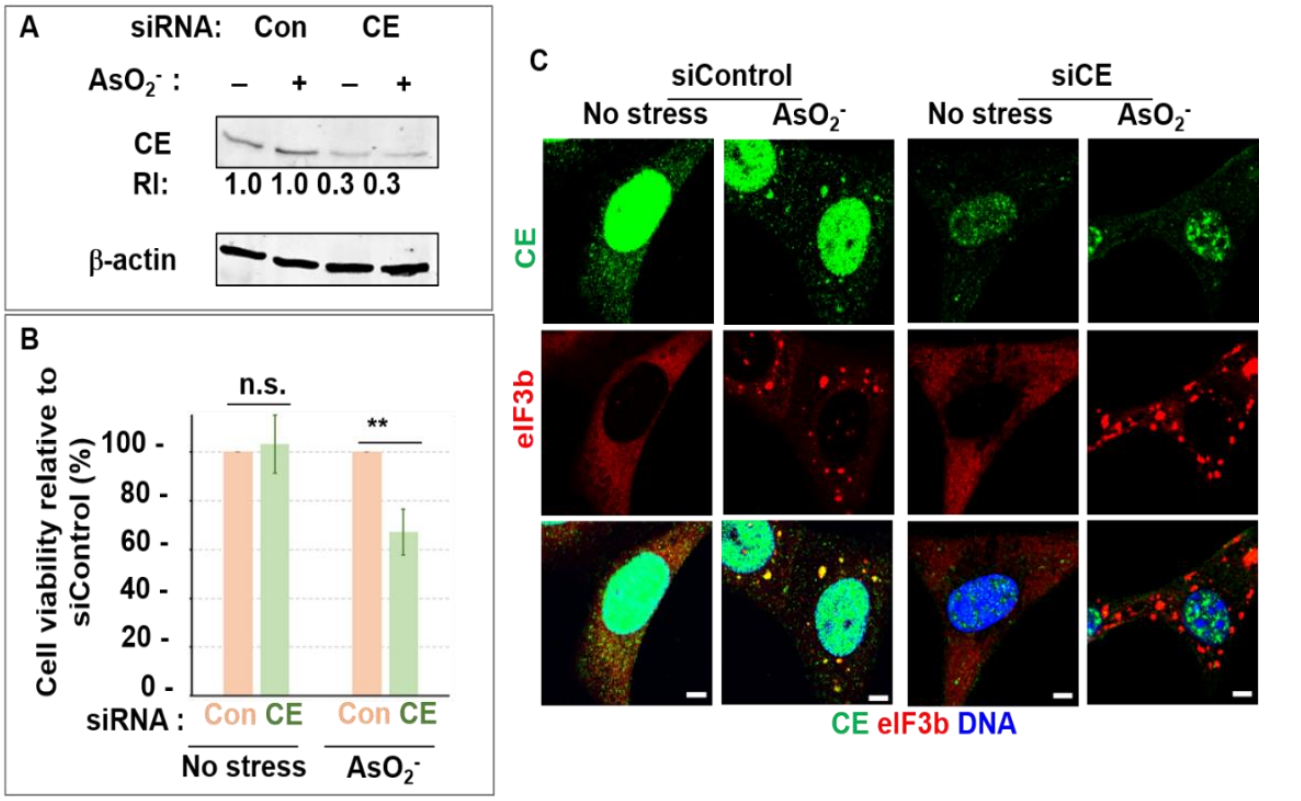

Fig5. ***SG formation remains unaltered upon CE depletion***. **(A)** Immunoblot analysis showing depletion of CE from U2OS cells in both non-stress and arsenite stress condition. In both the conditions, the level of protein reduction was almost 70% compared to control. **(B)** Cell viability assessment showing 30-40% reduction in cell viability when measured from sodium arsenite induced CE depleted cells compared to the uninduced one. **(C)** Confocal micrograph showing unaltered SGs in CE depleted cells. Bar represents 5 μM.

we depleted CE from U2OS cells using specific siRNA against CE. 10nM CE specific siRNA reduced the amount of protein by approximately 70%, analysed by Western hybridization (Fig 5A). As CE is indispensable for cells, a reduction in CE protein level followed by arsenite-stress resulted in 30-40% loss in cell viability (Fig 5B). A reduction of overall CE puncta was observed (Fig 5C). However, no alteration in size and number of eIF3 marked SGs was found when checked with indirect immunofluorescence. So, in conclusion, depletion of CE does not alter overall SG formation.

Overexpression of CE reduces SG formation

We have already observed that, depletion of CE from cells does not alter SG assembly (Fig 5C). In our docking approach we have identified that a significant number of amino acid residues of triphosphatase domain of CE form either hydrogen bonds or salt bridges or both with the amino acid residues of beta propeller domain of eIF3b compared to the guanylyl transferase domain (Fig 2G). To identify the domain required for SG recruitment the N-terminal TPase domain of CE was deleted and U2OS cells were transfected with myc-tagged CE-wt, CE-ΔTPase. To our surprise, we observed that the number of SGs were significantly reduced following the arsenite-treatment for both the transgene (Fig 6A) when ectopically-expressed (Fig 6B). As overexpression of CE inhibit SG formation, we tried to express CE in a regulated manner in the cell. We cloned myc tagged CE in pLVX Tet-one puro vector and transiently transfected U2OS cells, induced the exogenous protein at different doxycycline concentration followed by sodium arsenite treatment. Here interestingly most of the CE localized to nucleus. Few cells showed cytoplasmic localization of CE and those cells without cytoplasmic expression of CE formed SGs (Fig 6C). Expression was checked by Western blotting (Fig 6D). In conclusion, ectopic expression of myc-CE or myc-bio CE disrupt SG assembly.

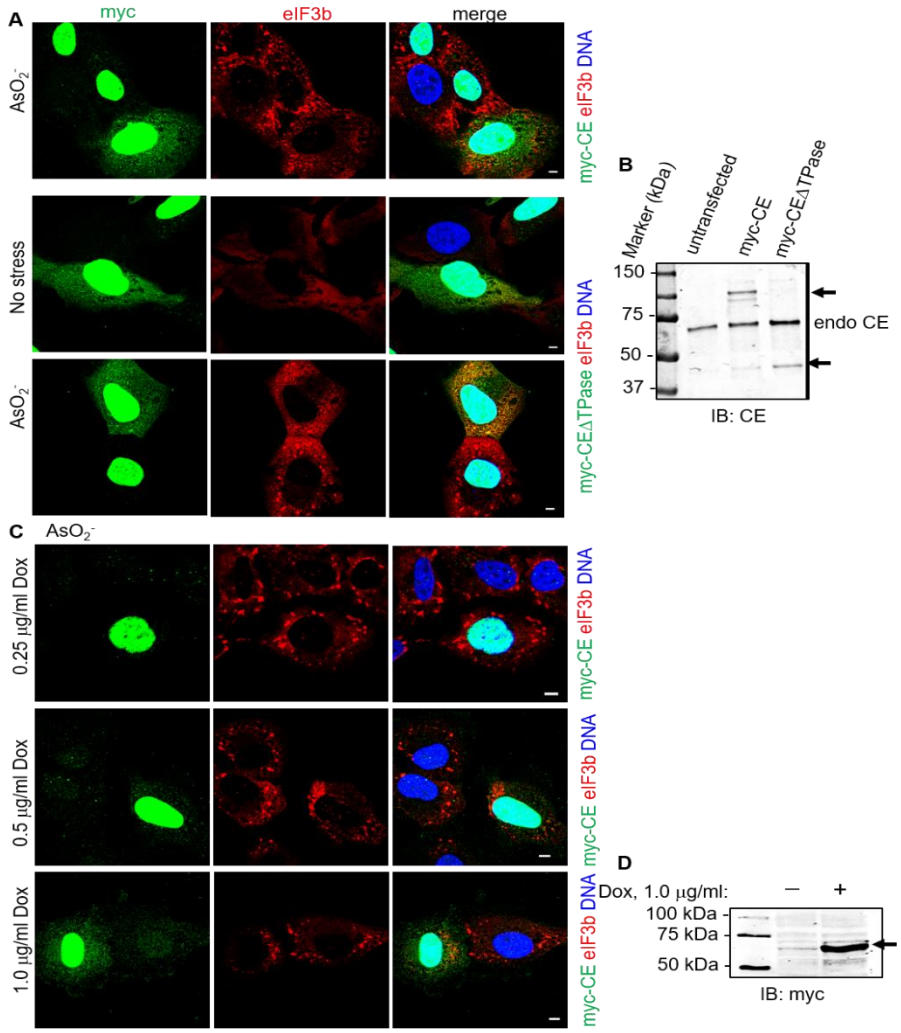

Fig6. ***Ectopic expression of CE reduces SG assembly.*** **(A)** Immunomicrograph showing formation of SGs reduced in myc tagged CE and CE-ΔTPase expressing cells. **(B)** Expression myc-CE and myc-CE ΔTPase by Western hybridization analysis. **(C)** Immunomicrograph of myc-CE expressed in a regulated manner using different concentration of doxycycline followed by induction of oxidative stress. **(D)** Western blot analysis of myc-CE with 1 µg/ml of doxycycline induction.

Recapped transcriptome helps cells to survive from oxidative stress

mRNAs containing Oligo Pyrimidine Motif (5'-TOP mRNAs) have also been identified as recapping target[31]. During stress, mRNAs are believed to lose their caps[32]. As our study discovered cCE as a resident of SGs, we speculated cCE might protect its' target transcripts during stress and restore the cap during removal from stress. So, we first checked the localization of cCE after stress removal and found cCE is dispersed to cytoplasm after 2 hrs of stress removal (Fig 7A). We then went ahead to check the capping

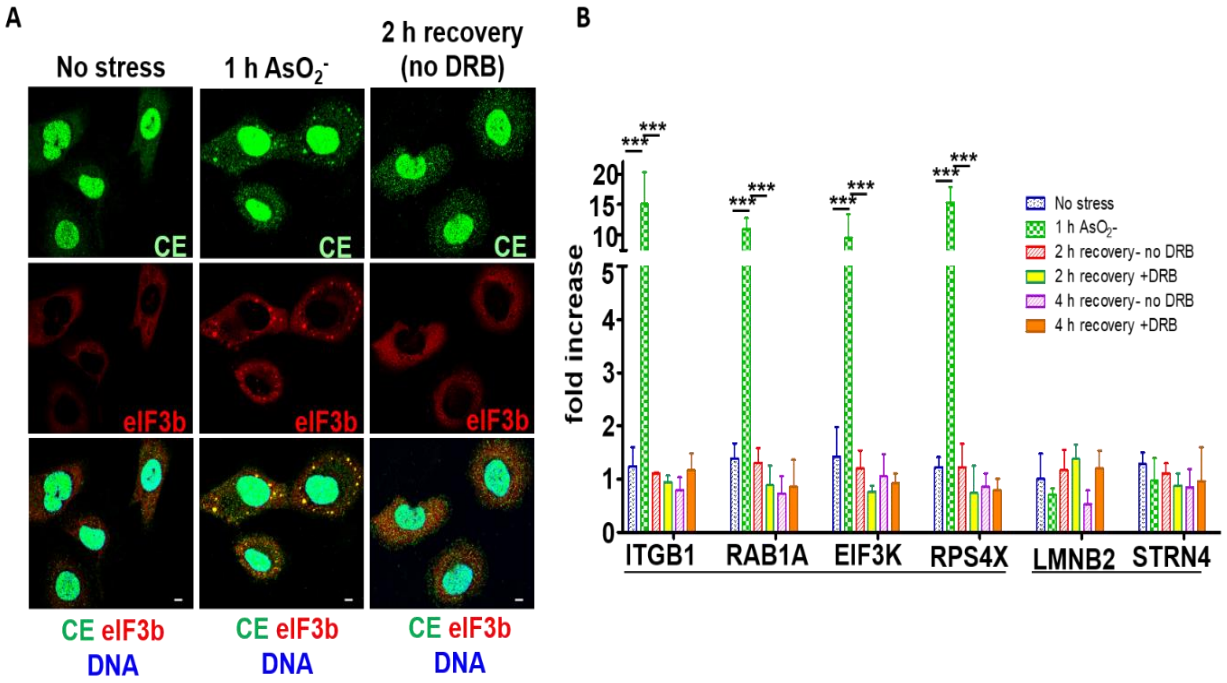

Fig7. ***Target transcripts gain cap structure during stress recovery***. **(A)** Immunofluorescence showing the dispersal of cCE after 2 hr of stress removal. **(B)** RT-qPCR analysis showing an increase in the uncapped mRNA level of target genes during oxidative stress compared to non-stress. Restoration of cap during recovery phase was identified as the level of uncapped transcripts decreases. *De novo* transcription was blocked by 10μM DRB.

status of cCE targets [such as ITGB1, RAB1A, EIF3K, RPS4X][31,10] and non-targets [such as LMNB2, STRN4]. At first, cytoplasmic RNA was isolated from different conditions followed by polyA selection. Next, *in vitro* Xrn1 digestion of polyA selected RNAs was performed to distinguish uncapped RNA from capped RNA and we observed recapping targets lost their caps in stress conditions compared to non-stress conditions, but regained the caps in recovery stage as evidenced by less susceptibility to Xrn1. However, no comparable change in cap status was observed in the case of non-targets (Fig 7B). Moreover, to inhibit *de novo* synthesis of mRNA during recovery, 10μM DRB, a transcription blocker was administered in a parallel experiment. No significant change was observed between DRB treated and untreated samples (Fig 7B). Overall, our study delineates that cCE acts in maintaining cap homeostasis of target mRNAs in cellular stress response.

Transcriptome wide analysis showed diabetes mellitus linked genes expressed differentially during stress recovery

Since, cCE maintains cap homeostasis of its' target mRNAs, thereby maintain cell survival, we sought to identify global change in the transcript level especially in stress recovery. U2OS line expressing K294A was induced with 1µg/ml doxycycline for 24 hrs. U2OS cells stably expressing TetR served as control.

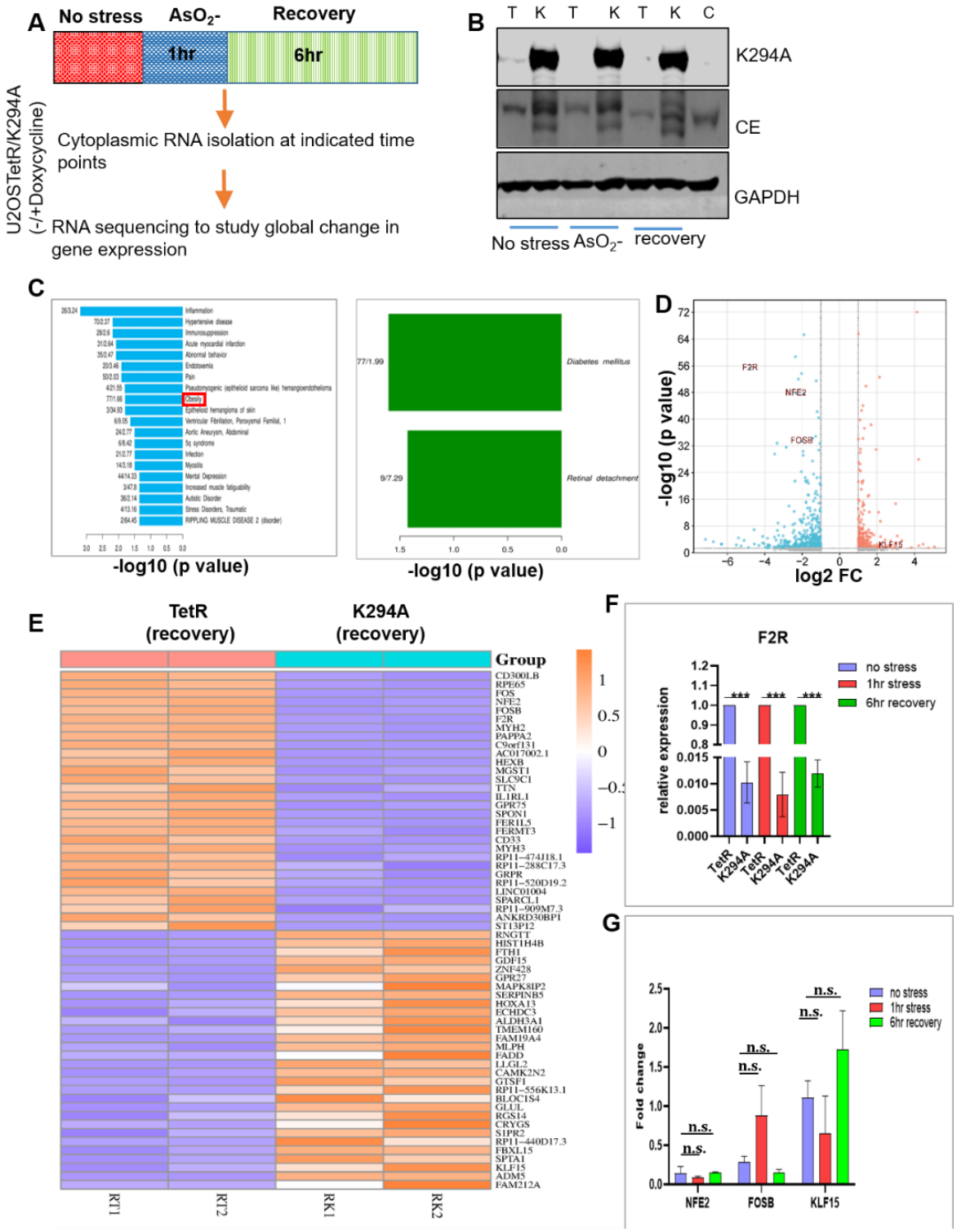

Fig8. *Differential gene expression analysis in recovery samples*. (A) Scheme of sample preparation for RNA sequencing analysis. **(B)** Expression of exogenous (K294A) and endogenous (CE) protein level. GAPDH used as control. **(C)** Disease ontology analysis showing differential expression of diabetes mellitus linked genes. **(D-E)** Volcano plot and heatmap showing differentially expressed genes. **(F-G)** Relative expression and fold change analysis of different up and downregulated genes.

Within this 24 hrs doxycycline induction span, cells were treated with 0.5 mM sodium arsenite to induce oxidative stress followed by 6 hrs of recovery (Fig 8A). Induction of Myc-K294A was checked by Western blot analysis (Fig 8B) and global change in mRNA level was determined by transcriptome wide sequencing analysis. Disease ontology enrichment analysis in recovery samples showed 77 genes which are related to diabetes mellitus are differentially expressed in K294A compared to TetR (Fig 8C). From these genes, three down regulated [F2R, NFE2, FOSB] and one upregulated gene [KLF15] with a fold change of 2 or more were selected for further validation (Fig 8D- G). However, due to technical issues this result remained inconclusive and needs further examination.

Objective3. Is CE-SG association regulated by VDACs?

cCE is present in the mitochondria

Mitochondria is one of the important organelles in the eukaryotic cells, which are responsible for energy production through ATP synthesis, maintaining calcium homeostasis, and regulating cellular apoptosis. Mitochondrial transcripts do not harbor a canonical m7G cap. However, a protein interactome analysis of CE identified a mitochondrial outer membrane protein voltage-dependent anion channel 3 (VDAC3) as an interactor in the cytoplasm among other mitochondrial proteins (Unpublished). Additionally, a recent study has unveiled that ROS production is elevated during long-term starvation when cells mostly rely on beta-oxidation of fatty acids for energy which in turn produces SGs. These SGs interact with mitochondrial membrane through mitochondrial porins[33]. These observations led us to think whether cCE regulates SGs through the interaction with mitochondria as ectopically expressing cCE reduces SG assembly (Fig 6A, 6C). To examine plausible mitochondrial targeting of cCE we looked for any mitochondrial target sequence (MTS) in CE using different prediction tools such as CELLO[34], DeepLoc-2.0[35], TargetP-2.0[36] and MitoFates[37]. However, the prediction scores for CE were much less when compared to the MTS of a mitochondrial-targeted protein TIM50 (Fig 9A). Next, immunostaining was carried out in U2OS and RPE1 cells using mitotracker-red, CoxIV (an inner mitochondrial membrane protein) and VDAC3 (Fig 9B-C). In each case, a few puncta of cCE were found to be localized with mitochondria. To further strengthen our observation, biochemical isolation of pure mitochondria was done from HEK293 cells and checked with different mitochondrial marker proteins such as VDAC1, TIM50, where β-actin was used as a negative control (9E). Based on previous information, we sought to

identify whether SG and mitochondria interact during oxidative stress. We found that, SGs and mitochondria come close during stress but do not overlap (Fig 9D).

A.

Prediction tools	Reference protein (TIM50)	CE
CELLO	1.898	0.205
DeepLoc-2.0	0.9236	0.0823
TargetP-2.0	0.996	0.049
MitoFates	1	0.012

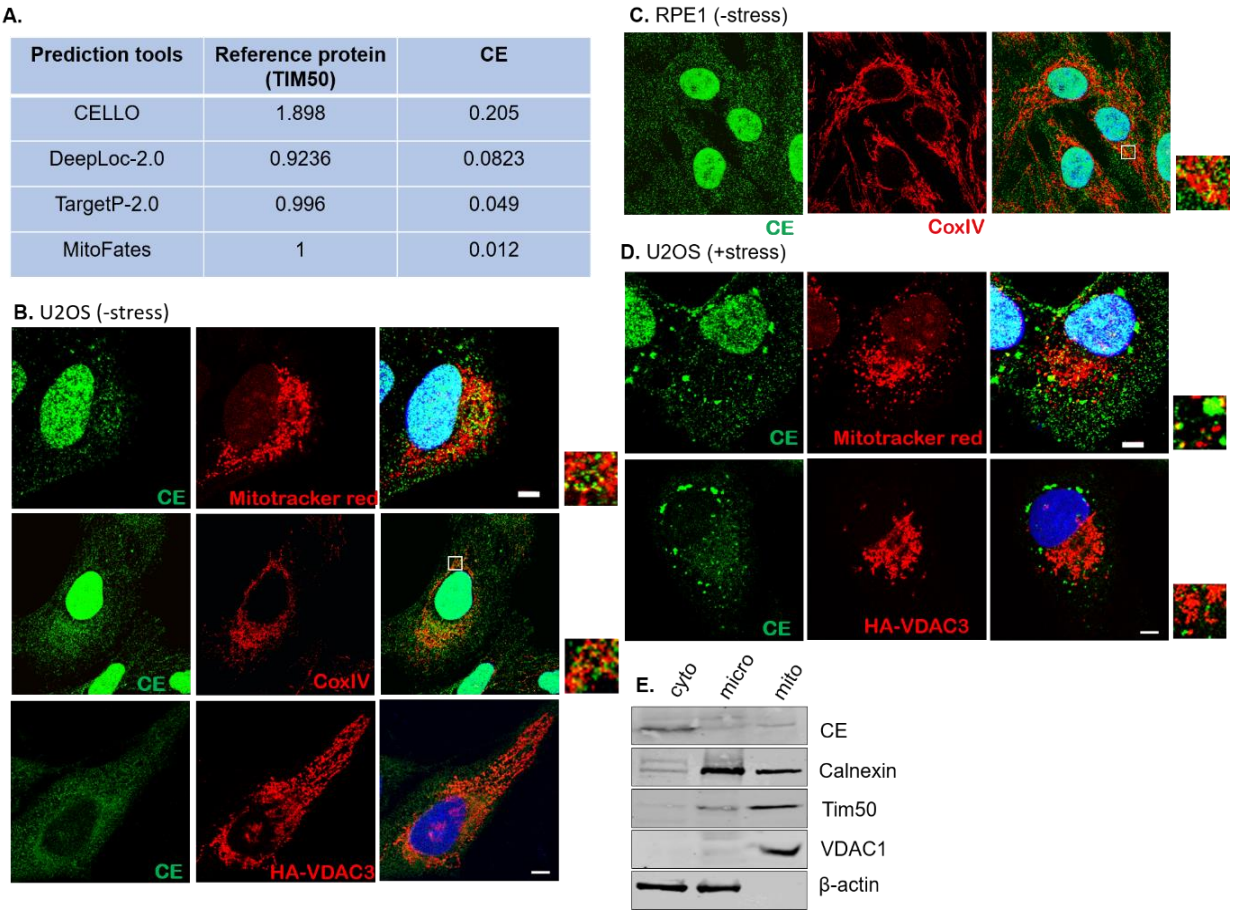

Fig9. *cCE localizes to mitochondria*. (A) Prediction tools showing less score for mitochondrial localization of CE when compared to a mitochondrial protein TIM50. **(B-C)** Immunostaining of U2OS and RPE1 with different mitochondrial markers. In each case a small pool of cCE localizes to mitochondria. **(D)** Immunofluorescence of U2OS cells after sodium arsenite treatment shows cCE containing SG puncta are in close proximity to the mitochondria. **(E)** Immunoblot analysis of isolated mitochondria, showing presence of cCE in it. Cyto- Cytplasmic fraction, Micro- Microsomal fraction, Mito- Mitochondrial fraction.

Mitochondrial porins interact with cCE and has an effect on SG dynamics

Voltage dependent anion channels (VDACs) are the most abundant proteins located on the outer membrane of mitochondria in eukaryotes as well as prokaryotes. They form channels bridging between mitochondria and cytosol in voltage sensitive manner, and play general function in exchanging small molecules and maintain the metabolic flux for cellular energy maintenance. Despite having similar sequences and structures, number of isoforms of VDACs differ in different organisms suggesting evolutionary divergence and different biological role of VDACs in normal and pathological conditions[38,39,40]. Mammalian VDACs have three isoforms originating from three different genes with different distributions in the cell and these isoforms show a quite similar structural organization with a

transmembrane region of barrel consisting of 19 amphipathic β-strands along with an N-terminal stretch of α-helix[41,42]. Previous study identified VDAC3 mRNA as a target of cCE[10]. We also found that VDAC2 mRNA but not VDAC1 mRNA could be regulated by cCE (Fig 10A). Interestingly, proteomics data suggests an interaction between VDAC3 and cCE (Unpublished). To validate that, ectopically expressing bio-myc CE and HA-VDAC3 were subjected to streptavidin pulldown. A non-interacting protein GFP tagged with HA (HA-GFP) was used as negative control. In addition, structural similarity among VDACs directed us to study the interaction of cCE with other two isoforms, VDAC 1 and VDAC2 and we found that in accordance with VDAC3, VDAC1 and VDAC2 also interact with cCE (Fig 10B). However, we limited to characterize the interaction between cCE and VDAC3 only due to its' specific function in redox signalling. Next, mitochondria was isolated after fractionation and similar pulldown using streptavidin and western hybridization analysis and out data showed interaction of VDAC3 with cCE majorly in the mitochondria instead of cytoplasm (Fig 10C).

Since cCE and VDAC3 interact in the mitochondria, we hypothesized that VDAC3 can be one of the cargos mediating the localization of cCE to the mitochondria. Therefore, we depleted VDAC3 from cells using specific siRNA against VDAC3 to visualize any alteration in the localization of cCE. Nonetheless, to our surprise, we found that upon VDAC3 depletion, size and number of SGs got reduced along with the cCE localization to SGs in both U2OS and RPE1cells (Fig 10D-E). Similarly, VDAC2 depletion but not VDAC1 depletion yielded the same phenotype (Fig 10D). Reduction in the VDACs mRNA level determined by RT-qPCR analysis (Fig 10F). Reduction in total fluorescence intensity of CE and eIF3b in eIF3b marked SGs in VDAC3 depleted cells (siVD3_CE and siVD3_eIF3) compared to the control (siC_CE and siC_eIF3) in both U2OS and RPE1 cells indicates an overall reduction of SGs (Fig 10G).

Discussion:

The first evidence of cytoplasmic capping was came to light when the decay intermediate of β-globin mRNA harboring a non-sense codon was resistant to 5'-3' exonuclease activity indicating the presence of 5'-cap termini[43]. In recent years, studies identified the presence of CE in the cytoplasm as to perform the main function in recapping the target transcripts[10,11] via the interaction with 5'-mono phosphate RNA kinase[8], an adaptor protein, NCK1[9] and RNA methyl transferase[44].

Our study first time showed the presence of CE in the cytoplasm (cCE) by indirect immunofluorescence assay. We also showed the presence of cCE in the mitochondria. In different studies, the biological function of cCE has been elucidated by the ectopic expression of myc-tagged CE-wt and K294A. We showed localization of endogenous CE using specific antibody of CE. To decipher the biological role of cCE, it's localization of cCE was first identified during stress with different SG markers eIF3b, TIA1, and G3BP1. Biochemical fractionation of SGs also showed the presence of cCE in the isolated SG fraction. However, cCE does not associate with the other RNP granule processing bodies (PBs) during both non-stress and stress conditions indicating the specific role of cCE in the cell survival since PBs are mostly

associated with RNA decay while SGs play a cytoprotective role during stress. This observation goes in line with our study that showed cCE helps in cellular survival from oxidative stress by recapping its' target transcripts during the recovery phase which can resonate with the fact that recapped transcripts are likely to enter the translating pool. Our data suggests, that upon eIF3b depletion, the number and size of SGs reduce resulting in decreased cCE localization to SGs. However, we could see a few cCE granules in the cytoplasm that do not localize with eIF3b marked SGs. So, there can be other mediators helping cCE to localize to SGs. However, our study clearly showed protective role of cCE in stabilizing its target transcripts during cellular recovery from arsenite-induced stress.

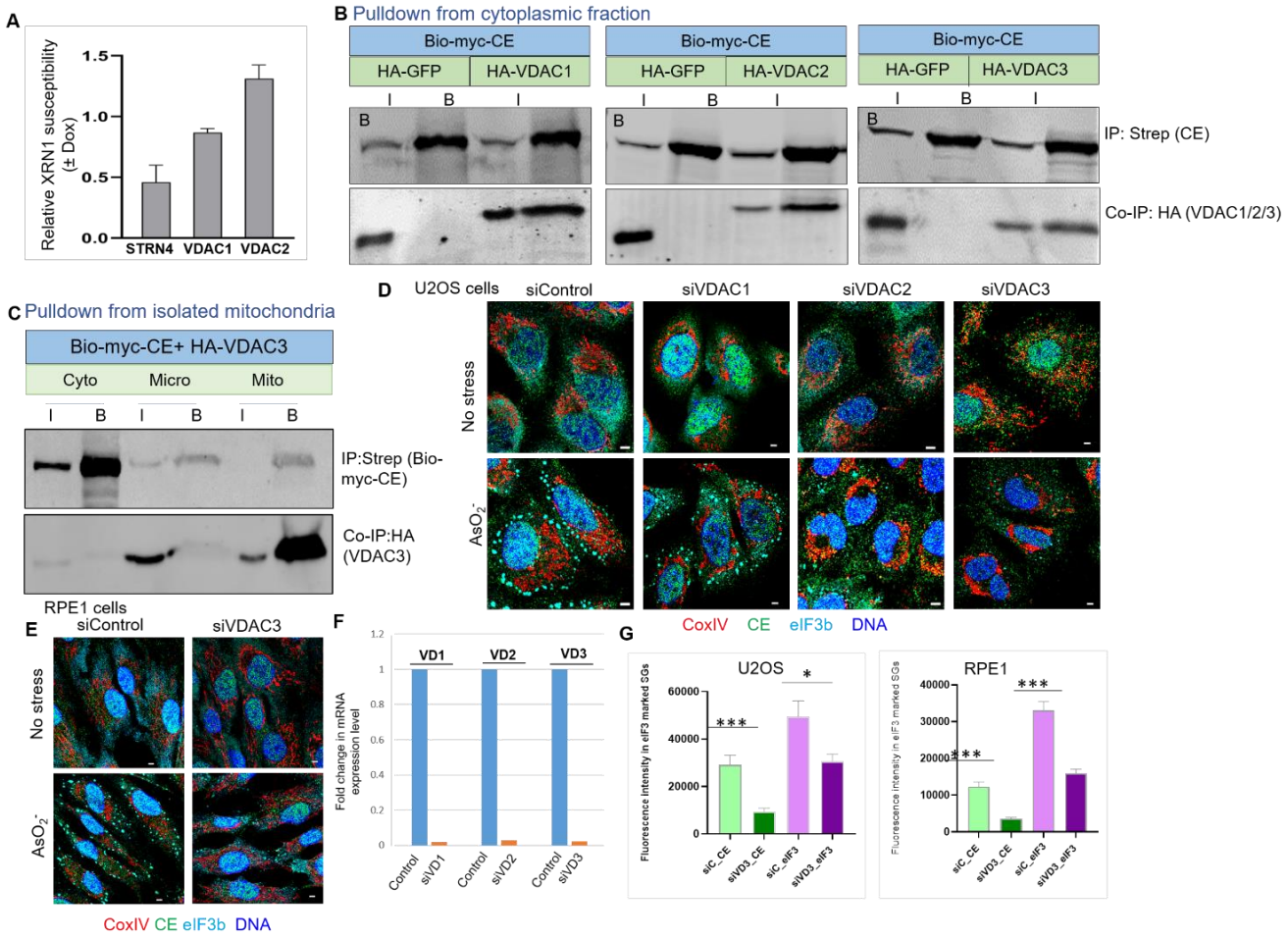

Fig 10. ***Interaction between cCE and VDACs.*** **(A)** Graph showing relative XRN1 susceptibility of VDAC1 and VDAC2 RNA of K294A expressing cells compared to non-target STRN4. **(B)** Streptavidin pulldown from cytoplasmic fraction of HEK293 cells co-transfected with bio-myc CE(wt) and HA-VDAC1/2/3 **(C)** Streptavidin pulldown from isolated pure mitochondria of HEK293 cells, co-transfected with bio-myc CE(wt) and HA-VDAC3. **(D)** Immunomicrograph showing reduction in SG number and size in VDAC2 and VDAC3 depleted cells, but not in VDAC1 depleted one. **(E)** Reduction of SG formation in RPE1 cells was seen when VDAC3 was depleted. **(F)** RT-qPCR analysis showing VDAC1,2,3 RNA level reduction upon siRNA treatment. **(G)** Total intensity of eIF3b and CE in the SGs reduced in VDAC3 depleted condition (siVD3_CE and siVD3_eIF3) when compared to control (siC_CE and siC_eIF3).

In search of the role of CE on SGs assembly, we depleted CE from cells using specific siRNA against CE and observation showed reduction of CE level does not alter the SG assembly. However, overexpression of CE-wt or cCE remarkably reduces SG formation. The mechanism behind this is still unclear. Transcriptome wide analysis of cytoplasmic RNA showed 77 genes that differentially expressed during stress recovery are associated with diabetes mellitus indicating a role of cCE in metabolism. Cellular metabolic processes occur in the mitochondria. Presence of cCE in the mitochondria and interaction with all the VDAC isoforms indicate its' role beyond recapping of target transcripts.

In conclusion, cCE is indispensable for cells to survive from oxidative stress through the recapping of its' target transcripts. Form RNA-sequencing analysis and form our observation it can be said that cCE might have a role in maintaining metabolic processes, but how cCE regulates metabolism and what effect cCE exactly repose on metabolism are need to be addressed. Future studies might focus on identifying the role of cCE in mitochondria. This study revealed like VDAC3mRNA, VDAC2 transcript can be regulated by cCE. Our study also opened up a novel function of VDACs in regulating SG assembly. Further studies should investigate the relationship between cCE and VDACs in regulating SG dynamics.

Bibliography

1. Furuichi, Y., Morgan, M., Muthukrishnan, S. & Shatkin, A. J. Reovirus messenger RNA contains a methylated, blocked 5' terminal structure: m7G(5')ppp(5')G(m)pCp. *Proc. Natl. Acad. Sci. U. S. A.* **72**, 362–366 (1975).
2. Cho, E. J., Takagi, T., Moore, C. R. & Buratowski, S. mRNA capping enzyme is recruited to the transcription complex by phosphorylation of the RNA polymerase II carboxy-terminal domain. *Genes and Development* vol. 11 3319–3326 (1997).
3. Ignatochkina, A. V., Takagi, Y., Liu, Y., Nagata, K. & Ho, C. K. The messenger RNA decapping and recapping pathway in Trypanosoma. *Proc. Natl. Acad. Sci. U. S. A.* **112**, 6967–6972 (2015).
4. Changela, A., Ho, C. K., Martins, A., Shuman, S. & Mondragón, A. Structure and mechanism of the RNA triphosphatase component of mammalian mRNA capping enzyme. *EMBO J.* **20**, 2575–2586 (2001).
5. Perry, R. P. & Kelley, D. E. Existence of methylated messenger RNA in mouse L cells. *Cell* **1**, 37–42 (1974).
6. Cowling, V. H. Regulation of mRNA cap methylation. *Biochem. J.* **425**, 295–302 (2010).
7. Lim, S., Mullins, J. J., Chen, C. M., Gross, K. W. & Maquat, L. E. Novel metabolism of several β°-thalassemic β-globin mRNAs in the erythroid tissues of transgenic mice. *EMBO J.* **8**, 2613–2619 (1989).
8. Otsuka, Y., Kedersha, N. L. & Schoenberg, D. R. Identification of a Cytoplasmic Complex That Adds a Cap onto 5′-Monophosphate RNA. *Mol. Cell. Biol.* **29**, 2155–2167 (2009).
9. Mukherjee, C., Bakthavachalu, B. & Schoenberg, D. R. The Cytoplasmic Capping Complex Assembles on Adapter Protein Nck1 Bound to the Proline-Rich C-Terminus of Mammalian Capping Enzyme. *PLoS Biol.* **12**, (2014).

10. Mukherjee, C. *et al.* Identification of Cytoplasmic Capping Targets Reveals a Role for Cap Homeostasis in Translation and mRNA Stability. *Cell Rep.* **2**, 674–684 (2012).

11. Mukherjee, A., Islam, S., Kieser, R. E., Kiss, D. L. & Mukherjee, C. Long noncoding RNAs are substrates for cytoplasmic capping enzyme. *FEBS Lett.* **597**, 947–961 (2023).

12. Riggs, C. L., Kedersha, N., Ivanov, P. & Anderson, P. Mammalian stress granules and P bodies at a glance. *J. Cell Sci.* **133**, 1–9 (2020).

13. Chen, L. & Liu, B. Relationships between Stress Granules, Oxidative Stress, and Neurodegenerative Diseases. *Oxid. Med. Cell. Longev.* **2017**, (2017).

14. Mo, Y. *et al.* Liquid–Liquid Phase Separation in Cardiovascular Diseases. *Cells* **11**, 1–14 (2022).

15. Zhou, H. *et al.* Stress granules: functions and mechanisms in cancer. *Cell Biosci.* **13**, 1–13 (2023).

16. Das, S., Santos, L., Failla, A. V. & Ignatova, Z. mRNAs sequestered in stress granules recover nearly completely for translation. *RNA Biol.* **19**, 877–884 (2022).

17. Wheeler, J. R., Jain, S., Khong, A. & Parker, R. Isolation of yeast and mammalian stress granule cores. *Methods* **126**, 12 (2017).

18. Schneidman-Duhovny, D., Inbar, Y., Nussinov, R. & Wolfson, H. J. PatchDock and SymmDock: Servers for rigid and symmetric docking. *Nucleic Acids Res.* **33**, 363–367 (2005).

19. Kozakov, D. *et al.* The ClusPro web server for protein-protein docking. *Nat. Protoc.* **12**, 255–278 (2017).

20. Yan, Y., Zhang, D., Zhou, P., Li, B. & Huang, S. Y. HDOCK: A web server for protein-protein and protein-DNA/RNA docking based on a hybrid strategy. *Nucleic Acids Res.* **45**, W365–W373 (2017).

21. Varadi, M. *et al.* AlphaFold Protein Structure Database: Massively expanding the structural coverage of protein-sequence space with high-accuracy models. *Nucleic Acids Res.* **50**, D439–D444 (2022).

22. Das, S. & Chakrabarti, S. Classification and prediction of protein–protein interaction interface using machine learning algorithm. *Sci. Rep.* **11**, 1–12 (2021).

23. Weng, G. *et al.* HawkDock: a web server to predict and analyze the protein-protein complex based on computational docking and MM/GBSA. *Nucleic Acids Res.* **47**, W322–W330 (2019).

24. Youn, J.-Y. *et al.* Molecular Cell Review Properties of Stress Granule and P-Body Proteomes. *Mol. Cell* **76**, 286–294 (2019).

25. Wagner, S., Herrmannová, A., Šikrová, D. & Valášek, L. S. Human eIF3b and eIF3a serve as the nucleation core for the assembly of eIF3 into two interconnected modules: the yeast-like core and the octamer. *Nucleic Acids Res.* **44**, 10772 (2016).

26. Ivanov, P., Kedersha, N. & Anderson, P. Stress granules and processing bodies in translational control. *Cold Spring Harb. Perspect. Biol.* **11**, (2019).

27. Trotman, J. B., Agana, B. A., Giltmier, A. J., Wysocki, V. H. & Schoenberg, D. R. RNA-binding proteins and heat-shock protein 90 are constituents of the cytoplasmic capping enzyme interactome. *J. Biol. Chem.* **293**, 16596–16607 (2019).

28. Yan, Y., Tao, H., He, J. & Huang, S. Y. The HDOCK server for integrated protein–protein docking. *Nat. Protoc.* **15**, 1829–1852 (2020).

29. 2023_eIF3 mRNA selectivity profiling reveals eIF3k as a cancer-relevant regulator of ribosome content.pdf.

30. Choi, Y. J., Lee, Y. S., Lee, H. W., Shim, D. M. & Seo, S. W. Silencing of translation initiation factor EIF3B promotes apoptosis in osteosarcoma cells. *Bone Jt. Res.* **6**, 186–193 (2017).

31. Del Valle Morales, D., Trotman, J. B., Bundschuh, R. & Schoenberg, D. R. Inhibition of cytoplasmic cap methylation identifies 5 top mrnas as recapping targets and reveals recapping sites downstream of native 5 ends. *Nucleic Acids Res.* **48**, 3806–3815 (2020).

32. Ehretsmann, C. P., Carpousis, A. J. & Krisch, H. M. messenger RNA Degradation in Procaryotes. *Faseb J* **6**, 3186–3192 (1992).

33. Amen, T. & Kaganovich, D. Stress granules inhibit fatty acid oxidation by modulating mitochondrial permeability. *Cell Rep.* **35**, (2021).

34. Yu, C. S. *et al.* CELLO2GO: A Web Server for Protein subCELlular LOcalization Prediction with Functional Gene Ontology Annotation. *PLoS One* **9**, e99368 (2014).

35. Thumuluri, V., Almagro Armenteros, J. J., Johansen, A. R., Nielsen, H. & Winther, O. DeepLoc 2.0: multi-label subcellular localization prediction using protein language models. *Nucleic Acids Res.* **50**, W228–W234 (2022).

36. Armenteros, J. J. A. *et al.* Detecting sequence signals in targeting peptides using deep learning. *Life Sci. Alliance* **2**, e201900429 (2019).

37. Fukasawa, Y. *et al.* MitoFates: improved prediction of mitochondrial targeting sequences and their cleavage sites. *Mol. Cell. Proteomics* **14**, 1113–1126 (2015).

38. Young, M. J., Bay, D. C., Hausner, G. & Court, D. A. The evolutionary history of mitochondrial porins. *BMC Evol. Biol.* **7**, (2007).

39. Wandrey, M., Trevaskis, B., Brewin, N. & Udvardi, M. K. Molecular and Cell Biology of a Family of Voltage-Dependent Anion Channel Porins in Lotus japonicus. *Plant Physiol.* **134**, 182–193 (2004).

40. Messina, A., Reina, S., Guarino, F. & De Pinto, V. VDAC isoforms in mammals. *Biochim. Biophys. Acta - Biomembr.* **1818**, 1466–1476 (2012).

41. Bayrhuber, M. *et al.* Structure of the human voltage-dependent anion channel. *Proc. Natl. Acad. Sci. U. S. A.* **105**, 15370–15375 (2008).

42. De Pinto, V. *et al.* Characterization of human VDAC isoforms: A peculiar function for VDAC3? *Biochim. Biophys. Acta - Bioenerg.* **1797**, 1268–1275 (2010).

43. Lim', S.-K. & Maquat2, L. E. Human beta-globin mRNAs that harbor a nonsense codon are degraded in murine erythroid tissues to intermediates lacking regions of exon I or exons I and II that have a cap-like structure at the 5' termini. *EMBO J.* **11**, 3271 (1992).

44. Trotman, J. B., Giltmier, A. J., Mukherjee, C. & Schoenberg, D. R. RNA guanine-7 methyltransferase catalyzes the methylation of cytoplasmically recapped RNAs. *Nucleic Acids Res.* **45**, 10726–10739 (2017).